energies

MDPI

Article

Numerical Study of Heat and Mass Transfer in the Original Structure and Homogeneous Substitution Model for Three Dimensional Porous Metal Foam

Hanbing Ke [1], Xuzhi Zhou [2], Tao Liu [3], Yu Wang [3] and Hui Wang [3,*]

[1] Science and Technology on Thermal Energy and Power Laboratory, Wuhan Second Ship Design and Research Institute, Wuhan 430205, China
[2] School of Power and Energy, Northwestern Polytechnical University, Xi'an 710072, China
[3] School of Aeronautics, Northwestern Polytechnical University, Xi'an 710072, China
* Correspondence: wanghui2018@nwpu.edu.cn

Abstract: In many applications, such as the miniaturization and cooling of high-power electronics in aerospace, a new thermal management solution is needed, and metal foam radiators may be a valuable solution. In this work, X-ray scanning was applied to obtain the original structure of the metal foam. The real structure calculation model of the metal foam was obtained through a series of modeling, and high-precision numerical simulation was built to study heat and mass transfer in the original structure and homogeneous substitution model for three-dimensional porous metal foam. The distribution of velocity, pressure and temperature field is investigated. The results show that the heat transfer characteristics increase and flow resistance decreases with an increase in the Reynolds number. The heat transfer performance and flow resistance increase with the decrease of porosity. The porous media homogenization model can be consistent with the original real calculation results of metal foam by using appropriate values of resistance coefficient and porosity. The variation of resistance coefficient and porosity with the working condition in the porous homogenization model is identified.

Keywords: metal foams; X-ray inspection; porous reconstruction; numerical simulation; homogeneous model

Citation: Ke, H.; Zhou, X.; Liu, T.; Wang, Y.; Wang, H. Numerical Study of Heat and Mass Transfer in the Original Structure and Homogeneous Substitution Model for Three Dimensional Porous Metal Foam. *Energies* **2023**, *16*, 1114. https://doi.org/10.3390/en16031114

Academic Editors: Dmitry Eskin and Gabriela Huminic

Received: 7 November 2022
Revised: 8 December 2022
Accepted: 16 December 2022
Published: 19 January 2023

1. Introduction

An example of a porous material with interconnected pores and a network made of metal skeletons connecting the solid phase is open-cell metal foam. It is strongly random in the immediate vicinity and somewhat uniform throughout. It has a very broad potential in applications where heat transmission needs to be improved because of its relatively high effective thermal conductivity, high surface area, and bending capabilities.

Currently, some researchers have investigated the flow and heat transfer properties of porous metal foams using numerical simulations of homogeneous models, simplified models, genuine structures, and real structures. For example, Gangapatnam et al. [1] reported on a numerical analysis of forced convection heat transport in highly porous aluminum foams. Numerical modeling is carried out while taking into account both local thermal equilibrium and nonlocal thermal equilibrium conditions. Dukhan et al. [2] has created a new geometric modeling of highly-porous, isotropic cellular media, such as open-cell metal. Due to fluid movement in very porous media, the modeling is only applicable for macroscopically two-dimensional heat transfer. In a metal-foam duct, forced convective heat transfer of a fluid (including nanoparticles) is explored numerically. For example, Xu et al. [3] obtains the velocity and temperature fields. Analysis is done on the impacts of a few significant parameters on the flow and heat transfer of nanofluid in porous media. Yao et al. [4] has looked at the characteristics of interfacial heat transmission

in metal foam porous media under a steady thermal conduction scenario. The relevant crucial heat flux data is gathered and examined. Arbak et al. [5] used a rectangular conduit filled with metal-foam and subjected to a steady heat flow on one side to study convective heat transfer. Comparing the performance of the foam to staggered pin fins with the same porosity and a diameter equivalent to the ligament of the foam allowed researchers to isolate the impact of the random orientation of the ligaments in the foam. The properties of oscillating water flow transmits heat in a commercial open-cell metal-foam pipe that Bagci experimentally discovered [6]. Gas and liquid flows in porous media differ primarily in how much dispersion matters in the latter. Kuruneru et al. [7] studied the flow of non-isothermal solid gas through an idealized metal foam heat exchanger. The heat and mass transfer characteristics in porous metal foams were investigated based on the characteristics of various solids. To conduct the experimental measurement for comprehending the forced airflow heat transfer behavior in open-cell porous foam, Xia et al. [8] designed a tubular apparatus packed with porous foam. An inverse analysis is used to calculate the volumetric heat transfer coefficients from the transient temperature data of airflow. Chen et al. [9] performed a three-dimensional numerical simulation to show the flow and heat transfer characteristics of a new tube bank design wrapped in metal foam. The effects of foam structural characteristics on heat transmission are examined. Xu et al. [10] used fractal grids to explain the pore structure of metal foams. The phase transition material in the cross-fractal metal foam is designed and numerically simulated as a two-dimensional unsteady melting model. Jang et al. [11] conducted a numerical evaluation of the effects of various operation circumstances and types of porous metal foams on the transport properties of the membrane humidifier. What changed to improve heat and mass transport was investigated. Li et al. [12] suggested partially filling the gas tube with metal foam to increase the gas' capacity for heat transfer while minimizing pressure loss. To examine the characteristics and impacts of this heat transfer enhancement technique, a wind tunnel-style gas heat transfer test equipment was constructed. Slimani et al. [13] studied the impact of the metal foam and the acoustic streaming produced by ultrasonic waves on heat transfer in forced convection in a heated plate. According to the findings, heat transmission is improved by both metallic foam and ultrasonic acoustic streaming separately. Different setups were compared in this study. Vazifeshenas et al. [14] addressed the impact of porous materials on heat transfer to the polymer electrolyte membrane fuel cells' traditional cooling channel. Due to fluid recirculation caused by randomly positioned tortuous ligaments, the heat transmission in these new channels is improved. Chen et al. [15] suggests combining a confined slot air jet and a bilayer aluminum foam block to improve heat transfer in the channel. The heat transmission in the metal foam block of the channel is greatly affected by the structural and operational characteristics. Rabbani et al. [16] studied the pressure drop and thermal performance in copper tubes partially filled with open-cell metal foams. The tubes are made by pouring liquid metal around a substance that serves as a space holder and has a porosity of 70%. Deng et al. [17] introduces the fractal Brownian motion to characterize the distribution of pores in porous metal foam. It is applied to examine the melting behaviors in porous metal foam with an emphasis on the function of pore distribution. Nilpueng et al. [18] describes a tiny copper foam-filled plate heat exchanger that can be used for small-scale electronic cooling. Experimental research is done on the heat transfer coefficient and pressure drop of water flowing inside a copper foam-filled plate heat exchanger. Additionally, the impact of water velocity and copper foam pore density on the best thermal performance is discussed. Arasteh et al. [19] used metal foam inserts partially in both pipes to examine the fluid flow and heat transfer in a double-pipe, counter-flow heat exchanger. The pipes were distributed with a constant volume of metal foam in the ideal way to maximize heat transfer while minimizing pressure drop increase. Mohammadpour-Ghadikolaie et al. [20] examined laminar forced convection heat transfer numerically from a constant temperature tube wrapped totally or partially by a metal porous layer and exposed to a uniform air cross flow. We considered how various novel configurations, where metal foam is simply used to cover a portion of the tube, might

perform thermally. Huisseune et al. [21] compares the performance of metal foam heat exchangers with that of a bare tube bundle and a currently used conventional louvered fin heat exchanger. Two-dimensional simulations on metal foam heat exchangers are carried out using a macroscopic model that combines the thermal non-equilibrium energy model with the Darcy-Forchheimer-Brinkman flow model. Zhang et al. [22] introduced the fractal to create the porous metal foam. An unsteady heat transfer model with solidification phase change in fractal porous metal foam embedded with phase change material is created and statistically investigated based on this fractal description. Wang et al. [23] examined the heat transfer and water flow properties in a copper foam tube, a nickel foam tube, and a smooth tube. A test is set up to check the efficiency of heat transmission and the flow properties of water in metal foam tubes, and copper and nickel foam tubes are made. Li et al. [24] conducted an experimental study on the heat transfer capabilities of water in the flow-boiling heat transfer process of several modified foam metal-filled channels. The foam metal has been treated in the experiment to increase its surface hydrophobicity, reduce its surface roughness, and stack its gradient pores. In order to increase the heat rate and reduce pumping power, Bianco et al. [25] numerically examined the thermo-fluid dynamics of both non-finned and finned metal foam heat sinks. A finite element was used to solve the governing equations, which could be formulated using the porous media theory under the assumptions of local thermal non-equilibrium. Trilok et al. [26] studied the cross relations among the morphological characteristics of stacked wire-mesh based on mesh-size, wire diameter and stacking type, which are essential for describing the medium and determining key input parameters required for numerical modeling. Shi et al. [27] reviewed the lasted advances in solid-liquid heat transfer in metal foams, and specifically analyzes the influencing factors on heat transfer performance as well as the mechanism of metal foam effects on heat transfer. Different optimized techniques for improving phase change heat transfer within metal foams and the current state of metal foam engineering applications for improving phase change heat transfer are reviewed and discussed.

As reviewed above, except for the experimental studies, which usually use a real porous metal foam structure, most numerical simulations use fractal or simplified structures. A fractal structure seems to be very complex and close to the real structure, but its essence is the periodic repetition of some micro-structure. It cannot reflect the randomness and inhomogeneity of the real structure. Using this structure costs a lot of computation expense, but it cannot obtain real and effective results. The simplified structures have similar problems. In this work, the original model is obtained by reconstructing the real metal foam structure, and accurate numerical simulation is carried out on the real structure model. Then, the feasibility of using the homogenized model to replace the original real structure is discussed, and the comparative calculation is carried out. Finally, the mathematical model of characteristic parameters of the homogenization model is given.

2. Physical Model and Reconstruction Method

Figure 1 shows both the original copper foam structure and the rebuilt structure. First, the complex porous structure is identified using X-ray computed tomography technology and image processing. The YXLON Cheetah X-ray inspection equipment scans the copper foam sample with a resolution of 25 μm. Then, a 3D model of a copper foam structure is restructured using Image J and Mimics Research. The metal foam surface is created using the 3D design and modeling program Mimics, and the skeleton micropore is then altered. We attempted to precisely characterize the skeleton's microporous structure and investigate how it affects the way mass and heat move. In the process of reconstructing the model, we processed a lot of small details to make the reconstructed microporous structure more like the original and simulateable. As shown in Table 1, the geometrical characteristics of the 3D model were calculated using the commercial programs Mimics and VG Studio. The porous interface will act as the boundary between porous media and water fluid.

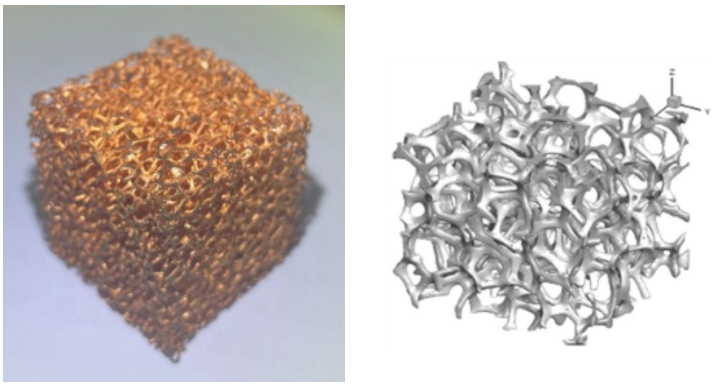

Figure 1. Original and reconstructed copper foam.

Table 1. Geometrical parameters of the porous model.

Dimension (mm^3)	Porosity	Pore Diameter (mm)	Structure Thickness (mm)
20 × 20 × 20	0.85, 0.90, 0.95	1.6~2.0	0.45~0.65

3. Mathematical Model

3.1. Governing Equations

It is assumed that the thermal contact resistance between the metal foam and the heat source is negligible. The heat source temperature is assumed to be constant because of the relatively high heat transfer coefficient of the heat sink. The metal foam surface temperature distribution will be determined by the conjugate heat transfer between the fluid and the solid. Since the air velocity is low and the porous channel is small, the air is considered as an incompressible fluid with constant physical properties.

Using the previously reconstructed pore-scale model, a quantitative analysis of the fluid flow and heat transfer in the copper foam porosity is performed. The fluid movement and heat transmission of the heat transfer fluid are governed by Equations (1)–(3). In the porous domain, heat transfer is described in Equation (4). The porous interface's coupled wall boundary condition enables heat transfer between the two domains.

$$\frac{\partial \rho}{\partial t} + \nabla \cdot (\rho \vec{V}) = S_m, \tag{1}$$

$$\frac{\partial}{\partial t}\left(\rho \vec{V}\right) + \nabla \cdot (\rho \vec{V}\vec{V}) = -\nabla p + \nabla \cdot (\bar{\bar{\tau}}) + \rho \vec{g} + \vec{F}, \tag{2}$$

$$\frac{\partial}{\partial t}(\rho E) + \nabla \cdot \left(\vec{V}(\rho E + p)\right) = \nabla \cdot \left(k_{eff}\nabla T - \sum_j h_j \vec{J}_j + \left(\bar{\bar{\tau}}_{eff} \cdot \vec{V}\right)\right) + S_h, \tag{3}$$

$$\frac{\partial}{\partial t}(\rho h) + \nabla \cdot \left(\vec{V}\rho h\right) = \nabla \cdot (k\nabla T) + S_h, \tag{4}$$

where p is the static pressure, τ is the stress tensor, and ρg is the gravitational body force. k_{eff} is the effective conductivity. The shear-stress transport (SST) k-ω model was used to solve turbulence.

$$\frac{\partial}{\partial t}(\rho k) + \nabla \cdot \left(\vec{v}\rho k\right) = \nabla \cdot (\Gamma_k \nabla k) + G_k - Y_k + S_k, \tag{5}$$

$$\frac{\partial}{\partial t}(\rho \omega) + \nabla \cdot \left(\vec{v}\rho \omega\right) = \nabla \cdot (\Gamma_\omega \nabla \omega) + G_\omega - Y_\omega + S_\omega, \tag{6}$$

In these equations, Γ_k and Γ_ω represent the effective diffusivity of k and ω, respectively. G_k represents the generation of turbulence kinetic energy due to mean velocity gradients.

G_ω represents the generation of ω. Y_k and Y_ω represent the dissipation of k and ω due to turbulence.

The discrete ordinates (DO) approach is used to resolve the thermal radiation transfer problem. In the process of heat transfer, it is important to take into account both the radiation energy absorbed by liquid media as well as the heat radiation exchanged between porous surfaces. Equation (7) describes the radiative transfer equation for a medium that emits, scatters, and absorbs radiation. The entire porous medium could be thought of as having a semi-transparent structure to thermal radiation.

$$\nabla \cdot \left(I_\lambda(\vec{r}, \vec{s})\vec{s} \right) + (\alpha_\lambda + \sigma_s) I_\lambda(\vec{r}, \vec{s}) = \alpha_\lambda n^2 I_{b\lambda} + \frac{\sigma_s}{4\pi} \int_0^{4\pi} I_\lambda(\vec{r}, \vec{s'}) \Phi(\vec{s}, \vec{s'}) d\Omega', \quad (7)$$

where r and s is the position and direction vector respectively. λ is the wavelength, α_λ is the spectral absorption coefficient, and $I_{b\lambda}$ is the black body intensity given by the Planck function. The scattering coefficient, the scattering phase function, and the refractive index n are assumed independent of wavelength. For non gray working medium, the radiation spectrum is divided into different wavelength bands for processing, and then superimposed the energy.

According to Momentum Equations for Porous Media, the homogeneous substitution model for porous media can establish a cell zone and calculate the pressure loss in the flow using the inputs. By including a momentum source factor in the common fluid flow equations, porous media are modeled. The source term is split into two components: An inertial loss term and a viscous loss term.

$$S_i = -\left(\frac{\mu}{\alpha} v_i + C_2 \frac{1}{2} \rho |v| v_i\right), \quad (8)$$

where S_i is the source term for the i (x, y, or z) momentum equation. a is the permeability and C_2 is the inertial resistance factor, respectively. The work of this paper is to predict these two parameters more accurately.

The homogenized model incorporates a synthetically determined flow resistance in a region defined as porous. This model adds a momentum sink in the governing momentum equations. Since the volume blockage that is physically present is not represented in the model, a superficial velocity inside the porous medium was used based on the volumetric flow rate, to ensure continuity of the velocity vectors across the porous medium interface. We used a more accurate alternative, in which the true velocity is calculated inside the porous medium and porosity is included in the differential terms of the transport equations.

3.2. Boundary Conditions

In the computing environment shown in Figure 2, where the thermal energy is put onto the side plane and the flow direction is parallel to the positive X coordinate axis. There is ample room for thermal equilibrium between the porous media and the heat transfer fluid with the entire length in the X direction is 20 mm.

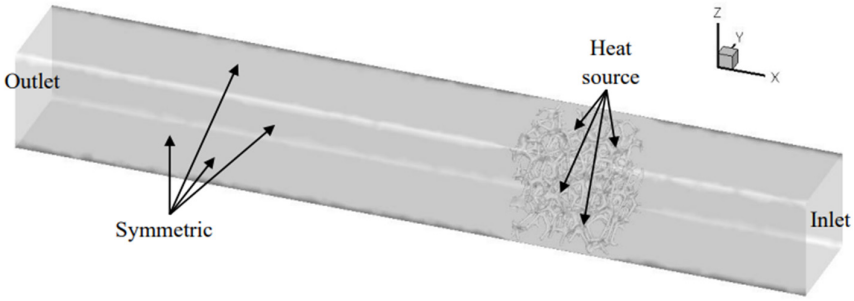

Figure 2. Compute region and boundary conditions.

To apply a uniform liquid medium velocity and temperature distribution at the domain's entrance, the computational domain is extended upstream by a length equal to the length of the copper foam. In order to apply an outflow boundary condition at the outlet, which is beyond any potential recirculation zone downstream of the porous model, the computational domain is extended downstream five times the length of the copper foam. The front surface is subjected to the constant temperature boundary condition and the mass flow input. The linked energy requirement is also satisfied, and the porous surface is provided an on-slip border.

When evaluating radiation transfer, the porous surface is regarded as opaque to radiation and emits thermal radiation with an emissivity of 0.95. It is believed that the liquid medium is transparent to radiation between two cut-off wave lengths, 5.2 m and 7.9 m. It attenuates radiation since it is opaque and has a very thin thickness.

3.3. Numerical Methods

Using the ICEM preprocessor, the required mesh is produced. A multiblock hybrid grid will be used. In order to capture the flow and heat transfer characteristics close to the foam skeleton surface, the grid is divided by local mesh refinement, and boundary layer grids are used in the fluid as close to the wall. The border layer has more than 20 grid layers, and the y+ of the first layer grid is less than 5. In Figure 3, the grid generation is displayed. Using Fluent 19.2, the governing equations are resolved. The physical property parameters were shown in Table 2. The finite volume method is used to discretize the governing equations. The coupled SIMPLE algorithm is used to solve the pressure and velocity coupling equations. The Eulerian model is applied to phase interaction problems. The momentum equation is discretized using the second-order up wind method. Increasing the mesh density and using second-order discrete method can effectively and significantly improve the influence of ray effect and false scattering, reduce the calculation error, and improve the calculation accuracy [28]. Due to the small pore scale of the porous metal foam used in our model, the mesh size is small in order to accurately describe the porous structure. In fact, in order to improve the calculation accuracy of heat transfer and flow characteristics, we use the second order discrete method. These setting also improves the calculation accuracy of radiation model. The convergence criteria for the momentum and continuity conservation equations are both less than 10^{-4}, whereas they are less than 10^{-6} for the energy equation.

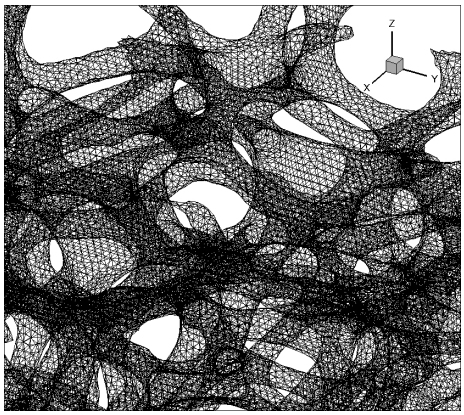

Figure 3. Grid of copper foam.

Table 2. Physical property parameter.

	Medium	**ρ (kg/m^3)**	**λ (W/m.K)**	**μ (kg/m.s)**
Solid	Copper	1800	245	/
Fluid	liquid medium	1.225	0.0242	1.7894×10^{-5}~1.7894×10^{-9}

3.4. Grid Independence

The construction is subjected to a grid independence test at a 10 m/s speed. Cursive refinement and comparison of the outcomes of the numerical simulation are used in the grid independence experiment. We choose and assess four different grid numbers. Table 3 presents the heat transfer rate for each grid. The adopted grid numbers are around 1.486×10^7 for numerical simulation, based on a thorough analysis of the computing accuracy and economics

Table 3. Results of different grid numbers.

Grid Number	$\mathbf{1.228 \times 10^7}$	$\mathbf{1.351 \times 10^7}$	$\mathbf{1.486 \times 10^7}$	$\mathbf{1.635 \times 10^7}$
Nu	237.51	244.98	247.12	247.63

4. Results and Discussion

4.1. Flow and Heat Transfer of Original Structures

Figure 4 shows the relative pressure distribution diagram of the original real metal foam porous media. As can be seen in the figure, a certain pressure drop occurs when the fluid flows through the porous metal foam. This is because the presence of metal foam skeleton, the boundary layer near the skeleton surface will continue to expand downstream from the upwind surface of the metal foam, causing flow resistance. At the same time, due to the small scale of the channel inside the metal foam, the fluid will produce resistance due to viscosity. In addition, the metal foam skeleton has a blocking effect on the flow, and various factors jointly affect the flow, resulting in a pressure drop loss when the fluid passes through the metal foam. Due to the great randomness of the structure inside the metal foam, the probability that a certain position inside the foam is a void or a metal skeleton depends on the total porosity. Due to the randomness of the metal foam structure and the uniformity of probability, the flow resistance and pressure loss can be calculated by the homogenization model instead of the real model.

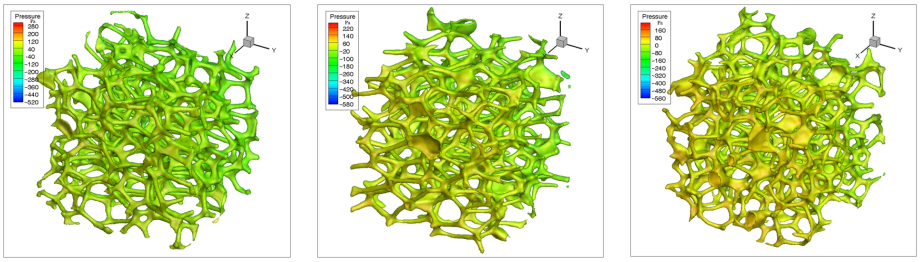

Figure 4. Overall relative pressure distribution.

Figure 5 shows the temperature distribution of the original real metal foam porous media. It can be seen from the figure that the temperature of the fluid rises obviously after flowing through the porous metal foam with a high temperature wall. On the one hand, the heat from the surrounding wall will be transferred to the inside of the metal foam through the metal skeleton with high thermal conductivity, and then the heat will be transferred to the fluid by the convective heat transfer between the fluid and the metal skeleton wall. On the other hand, the heat will be directly transferred to the fluid through heat conduction and convection from the walls. In addition, the mutual radiation between the metal foam skeletons will also affect the heat transfer and temperature distribution. A combination of factors causes the fluid to gain heat as it passes through the metal foam, resulting in an increase in temperature. While the structure of the metal foam is random, the heat transfer is different from the flow resistance, which is transferred from the surrounding to the center and from the wall to the fluid. Therefore, the value of parameters, especially porosity, may be different from that of the real metal foam when the homogenization model is used instead of the real model to calculate heat transfer. It is necessary to obtain the relationship

between the porosity value of homogenization model and the real parameters and operating parameters through theoretical analysis and a large number of design calculations.

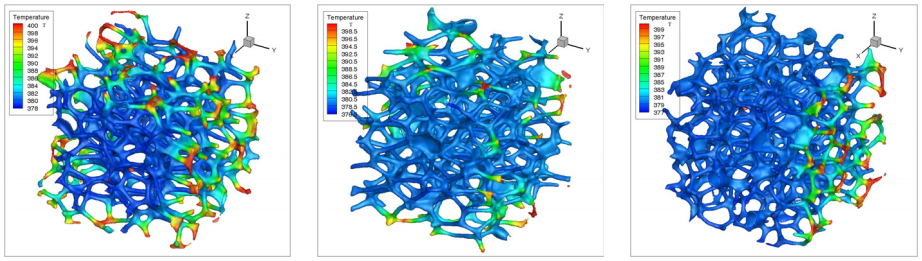

Figure 5. Global temperature distribution.

Figure 6 shows the distribution of velocity, relative pressure and temperature in the middle section of the original real metal foam porous media. As can be seen in the figure, when the fluid flows through the metal foam skeleton, low velocity areas will be formed near and downstream of the skeleton. There are significant pressure changes in the upstream and downstream regions of the skeleton. The temperature of the skeleton near the side is higher, while the temperature of the inner skeleton is lower. A large amount of heat is transferred by convective heat transfer on the skeleton surface. These phenomena and processes are consistent with the previously analyzed mechanisms of heat transfer and flow resistance.

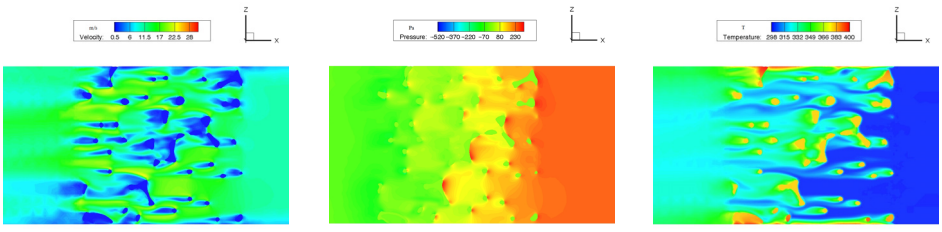

(**a**) Porous 0.95

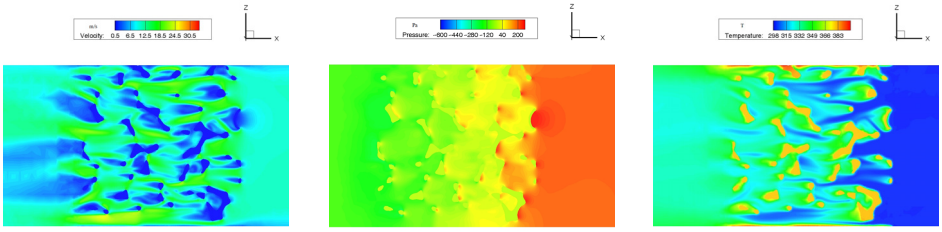

(**b**) Porous 0.90

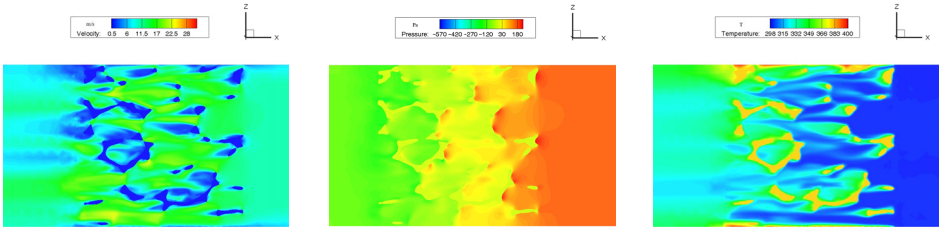

(**c**) Porous 0.85

Figure 6. Velocity, pressure and temperature distribution in the middle section of the model.

Figure 7 shows the variation of the numerical simulation results of the original real metal foam porous medium with Re number, and Figure 7a shows the variation of the heat transfer characteristics with Re number. With the increase of Re number, *Nu* number,

which represents the thermal property of heat transfer, also increases, and the slope of the increase first increases and then decreases. When Re number is small, increasing Re number can significantly enhance heat transfer. When Re number is large, the heat transfer capacity tends to be saturated. The strengthening effect of increasing Re number on heat transfer performance decreased. Figure 7b shows the variation of flow resistance characteristics with Re number. According to the actual application background, we adopt the method of reducing the viscosity to increase the Re number, and the flow of the inlet remains unchanged. Under these conditions, with the increase of Re number, the f number representing the thermal property of flow resistance decreases, and the decreasing rate shows a decreasing trend. In general, the larger the porosity, the larger the fluid flow area, and the smaller the solid skeleton area of the metal foam. Therefore, the heat transfer performance and flow resistance increase with the decrease of porosity.

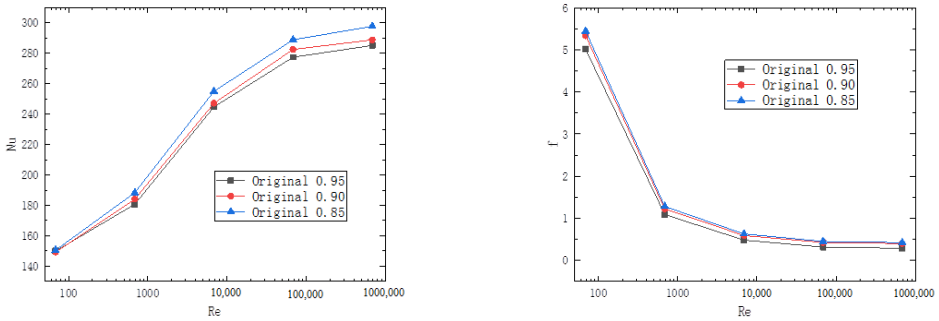

(**a**) Heat transfer characteristics (**b**) Flow resistance characteristics

Figure 7. Heat transfer and flow resistance characteristics.

4.2. Comparison of Equivalent Homogenization Models

As the original real porous structure of metal foams is very complex, difficult to calculate, long cycle, and high cost, the porous media homogenization equivalent model is used for alternative calculation. When using the homogeneous equivalent model of porous media, two important parameters, resistance coefficient and porosity, should be given. The resistance coefficient affects the velocity and pressure variation of the fluid passing through the porous media homogenization model, which also affects the heat transfer characteristics. The porosity affects the overall thermal physical properties of porous media homogenization model and the heat transfer performance. According to the previous analysis, both the resistance coefficient and porosity need to be calculated through a mathematical model, which is half theoretical and half empirical, and this mathematical model requires extensive design calculations to obtain. Figure 8 shows the comparison results of heat transfer and flow resistance characteristics between the original structure and the homogenized model. It can be seen from the comparison figure that the calculation results of porous media homogenization model can be consistent with the original real calculation results of metal foam by using appropriate values of the resistance coefficient and porosity.

Through a large number of designed calculations, the calculation results of the homogenization model, as shown in Figure 8, have a small error with the original metal foam structure. Figure 9 shows the variation of resistance coefficient and porosity with the working condition in the porous homogenization model. Through the equation regression, we can obtain the mathematical model of the drag coefficient and porosity value.

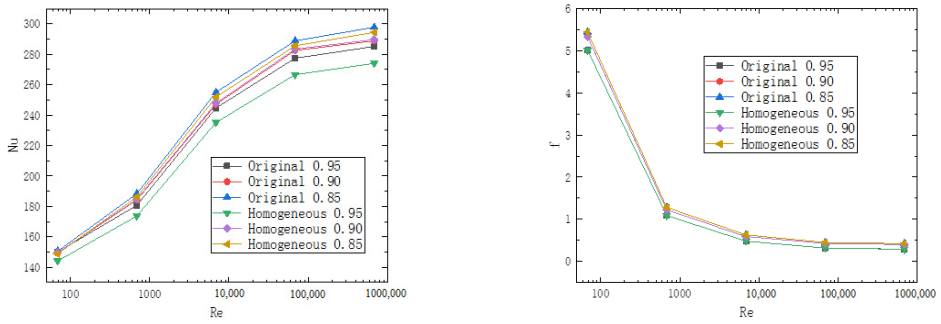

(**a**) Heat transfer characteristics (**b**) Flow resistance characteristics

Figure 8. Comparison between the original structure and the homogenized model.

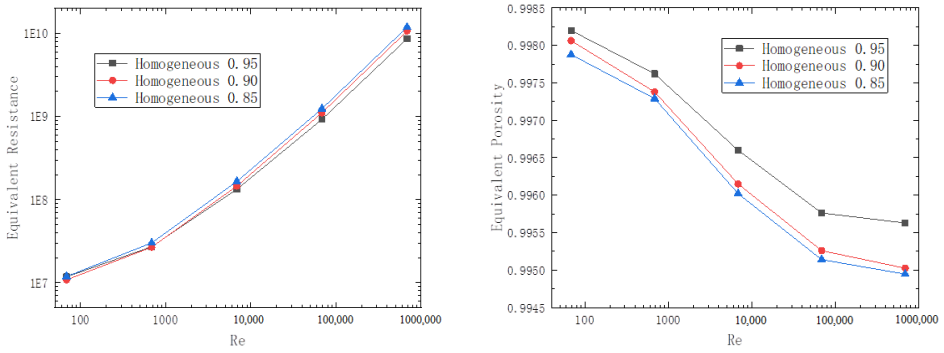

(**a**) Resistance coefficient (**b**) Porosity variation

Figure 9. Variation of resistance coefficient and porosity of the porous homogenization model.

5. Conclusions

In this paper, X-ray scanning is used to obtain the original structure of the metal foam, and the real structure calculation model of the metal foam is obtained through a series of modeling, and high precision numerical simulation is carried out. The homogenization equivalent model of porous media is used to calculate. X-ray scanning was used to obtain the original structure of the metal foam, and the real structure calculation model of the metal foam was obtained through a series of modeling, and high-precision numerical simulation was carried out. The real metal foam structure is numerically studied, the distribution of velocity, pressure and temperature field is studied, the change law of the heat transfer and flow characteristics is analyzed, and the feasibility of alternative calculation by homogenized equivalent model is discussed. The homogenization equivalent model of porous media was established, and the appropriate values of drag coefficient and porosity were obtained through reasonable design and calculation, and the simulation results of the original structure were compared, and the mathematical model of drag coefficient and porosity was regressed. The calculation results of porous media homogenization model can be consistent with the original real calculation results of metal foam by using appropriate values of the resistance coefficient and porosity. The variation of resistance coefficient and porosity with the working condition in the porous homogenization model is distinguished.

Author Contributions: H.K.: Methodology, Validation, Formal analysis, Investigation, Writing—original draft. X.Z.: Methodology, Validation, Formal analysis, Investigation, Writing—original draft. T.L.: Writing—review & editing, Supervision, Y.W.: Review & editing, Formal analysis. H.W.: Review & editing, Formal analysis, Project administration. All authors have read and agreed to the published version of the manuscript.

Funding: This work has been supported by the Open Fund of the Key Laboratory of Thermal Power Technology (No. TPL2019B02), This research received no external funding.

Data Availability Statement: Not applicable.

Conflicts of Interest: The authors declare no conflict of interest.

Nomenclature

f	Friction resistance value $f = \Delta p(L/D)/(0.5\rho v^2)$
Nu	Nusselt number $Nu = hL/k$
p	Static pressure (Pa)
T	Temperature (K)
V	Velocity (m/s)
Greek symbols	
ρ	Density (kg/m^3)
λ	Effective thermal conductivity [W/(m·K)]
μ	Work medium dynamic viscosity [kg/(m·s)]
τ	Stress tensor
φ	Volumetric concentration (%)

References

1. Gangapatnam, P.; Kurian, R.; Venkateshan, S.P. Numerical simulation of heat transfer in metal foams. *Heat Mass Transf.* **2018**, *54*, 553–562. [CrossRef]
2. Dukhan, N. Equivalent Parallel Strands Modeling of Highly-Porous Media for Two-Dimensional Heat Transfer: Application to Metal Foam. *Energies* **2021**, *14*, 6308. [CrossRef]
3. Xu, H.J.; Gong, L.; Huang, S.B. Flow and heat transfer characteristics of nanofluid flowing through metal foams. *Int. J. Heat Mass Transf.* **2015**, *83*, 339–407. [CrossRef]
4. Yao, Y.P.; Wu, H.Y. Interfacial heat transfer in metal foam porous media (MFPM) under steady thermal conduction condition and extension of Lemlich foam conductivity theory. *Int. J. Heat Mass Transf.* **2021**, *169*, 120974. [CrossRef]
5. Arbak, A.; Dukhan, N. Performance and heat transfer measurements in asymmetrically-heated metal foam cooled by water. *Therm. Sci. Eng. Prog.* **2020**, *20*, 100688. [CrossRef]
6. Bagci, O.; Dukhan, N.; Ozdemir, M.; Kavurmacioglu, L.A. Experimental heat transfer due to oscillating water flow in open-cellmetal foam. *Int. J. Therm. Sci.* **2016**, *101*, 48–58. [CrossRef]
7. Kuruneru, S.T.W.; Saha, S.C.; Sauret, E.; Gu, Y.T. Transient heat transfer and non-isothermal particle-laden gas flows through porous metal foams of differing structure. *Appl. Therm. Eng.* **2019**, *150*, 888–903. [CrossRef]
8. Xia, X.L.; Chen, X.; Sun, C.; Li, Z.H.; Liu, B. Experiment on the convective heat transfer from airflow to skeleton in open-cell porous foams. *Int. J. Heat Mass Transf.* **2017**, *106*, 83–90. [CrossRef]
9. Chen, K.; Wang, X.; Chen, P.F.; Wen, L. Numerical simulation study on heat transfer enhancement of a heat exchanger wrapped with metal foam. *Energy Rep.* **2022**, *8*, 103–110. [CrossRef]
10. Xu, H.; Yao, F.; Zhang, C.B. Numerical study on melting heat transfer in fractal metal foam. *Fractals-Complex Geom. Parrtens Scaling Nat. Soc.* **2019**, *27*, 1950106. [CrossRef]
11. Jang, H.; Kim, M.H.; Park, S.K.; Kim, Y.S.; Choi, B.C. Simulation of Heat and Mass Transfer Characteristics for the Optimal Operating Conditions of a Gas-to-Gas Membrane Humidifier with Porous Metal Foam. *Energies* **2020**, *13*, 5110. [CrossRef]
12. Li, Y.Z.; Wang, S.X.; Zhao, Y.L. Experimental study on heat transfer enhancement of gas tube partially filled with metal foam. *Exp. Therm. Fluid Sci.* **2018**, *97*, 408–416. [CrossRef]
13. Slimani, L.; Hamadouche, A.; Bousri, A.; Ben Hamed, H. Heat transfer enhancement using 40 kHz ultrasound and metal foams inside a horizontal mini-channel. *Appl. Therm. Eng.* **2022**, *216*, 119039. [CrossRef]
14. Vazifeshenas, Y.; Sedighi, K.; Shakeri, M. Heat transfer in PEM cooling flow field with high porosity metal foam insert. *Appl. Therm. Eng.* **2019**, *147*, 81–89. [CrossRef]
15. Chen, W.; Li, L.X. Analysis of heat transfer in a bilayer metal foam block subjected to an impinging air jet. *Heat Transf. Res.* **2017**, *48*, 1281–1298. [CrossRef]
16. Rabbani, P.; Hamzehpour, A.; Ashjaee, M.; Najafi, M.; Houshfar, E. Experimental investigation on heat transfer of MgOnanofluid in tubes partially filled with metal foam. *Power Technol.* **2019**, *354*, 734–742. [CrossRef]
17. Deng, Z.L.; Liu, X.D.; Zhang, C.B.; Huang, Y.P.; Chen, Y.P. Melting behaviors of PCM in porous metal foam characterized by fractal geometry. *Int. J. Heat Mass Transf.* **2017**, *113*, 1031–1042. [CrossRef]
18. Nilpueng, K.; Asirvatham, L.G.; Dalkilic, A.S.; Mahian, O.; Ahn, H.S.; Wongwises, S. Heat transfer and fluid flow characteristics in a plate heat exchanger filled with copper foam. *Heat Mass Transf.* **2020**, *56*, 3261–3271. [CrossRef]
19. Arasteh, H.; Salimpour, M.R.; Tavakoli, M.R. Optimal distribution of metal foam inserts in a double-pipe heat exchanger. *Intern. J. Numer. Methods Heat Fluid* **2019**, *29*, 1322–1342. [CrossRef]
20. Mohammadpour-Ghadikolaie, M.; Saffar-Avval, M.; Mansoori, Z.; Alvandifar, N.; Rahmati, N. Heat Transfer Investigation of a Tube Partially Wrapped by Metal Porous Layer as a Potential Novel Tube for Air Cooled Heat Exchangers. *J. Heat Transf.-Trans. ASME* **2019**, *141*, 011802. [CrossRef]

21. Huisseune, H.; De Schampheleire, S.; Ameel, B.; De Paepe, M. Comparison of metal foam heat exchangers to a finned heat exchanger for low Reynolds number applications. *Int. J. Heat Mass Transf.* **2015**, *89*, 1–9. [CrossRef]
22. Zhang, C.B.; Wu, L.Y.; Chen, Y.P. Study on solidification of phase change material in fractal porous metal foam. *Fractals- Complex Geom. Patterns Scaling Nat. Soc.* **2015**, *3*, 1540003. [CrossRef]
23. Wang, G.Q.; Qi, C.; Pan, Y.H.; Li, C.Y. Experimental study on heat transfer and flow characteristics of two kinds of porous metal foam tubes filled with water. *Therm. Sci.* **2018**, *22*, 497–505. [CrossRef]
24. Li, H.W.; Chang, T.L.; Du, C.H.; Fu, D.W.; Hong, W.P. Experimental study on flow boiling heat transfer characteristics of multi-channel modified filled foam metal small channel. *Int. Commun. Heat Mass Transf.* **2021**, *127*, 105588. [CrossRef]
25. Bianco, N.; Iasiello, M.; Mauro, G.M.; Pagano, L. Multi-objective optimization of finned metal foam heat sinks: Tradeoff between heat transfer and pressure drop. *Appl. Therm. Eng.* **2021**, *182*, 116058. [CrossRef]
26. Trilok, G.; Kurma, E.S.S.; Devika, H.; Gnanasekaran, N.; Moghtada, M. Correlations and Numerical Modeling of Stacked Woven Wire-Mesh Porous Media for Heat Exchange Applications. *Energies* **2022**, *15*, 237.
27. Shi, J.; Du, H.Y.; Chen, Z.Q.; Lei, S.Y. Review of phase change heat transfer enhancement by metal foam. *Appl. Therm. Eng.* **2023**, *219*, 119427. [CrossRef]
28. Moghimi, M.A.; Craig, K.J.; Meyer, J.P. A novel computational approach to combine the optical and thermal modelling of Linear Fresnel Collectors using the finite volume method. *Sol. Energy* **2015**, *216*, 407–427. [CrossRef]